Scale dependence of deuteron electrodisintegration

S. N. More,[1,*] S. K. Bogner,[1,†] and R. J. Furnstahl[2,‡]
[1]*National Superconducting Cyclotron Laboratory and Department of Physics and Astronomy, Michigan State University, East Lansing, Michigan 48824, USA*
[2]*Department of Physics, The Ohio State University, Columbus, Ohio 43210, USA*
(Received 19 August 2017; published 20 November 2017)

Background: Isolating nuclear structure properties from knock-out reactions in a process-independent manner requires a controlled factorization, which is always to some degree scale and scheme dependent. Understanding this dependence is important for robust extractions from experiment, to correctly use the structure information in other processes, and to understand the impact of approximations for both.
Purpose: We seek insight into scale dependence by exploring a model calculation of deuteron electrodisintegration, which provides a simple and clean theoretical laboratory.
Methods: By considering various kinematic regions of the longitudinal structure function, we can examine how the components—the initial deuteron wave function, the current operator, and the final-state interactions (FSIs)—combine at different scales. We use the similarity renormalization group to evolve each component.
Results: When evolved to different resolutions, the ingredients are all modified, but how they combine depends strongly on the kinematic region. In some regions, for example, the FSIs are largely unaffected by evolution, while elsewhere FSIs are greatly reduced. For certain kinematics, the impulse approximation at a high renormalization group resolution gives an intuitive picture in terms of a one-body current breaking up a short-range correlated neutron-proton pair, although FSIs distort this simple picture. With evolution to low resolution, however, the cross section is unchanged but a very different and arguably simpler intuitive picture emerges, with the evolved current efficiently represented at low momentum through derivative expansions or low-rank singular value decompositions.
Conclusions: The underlying physics of deuteron electrodisintegration is scale dependent and not just kinematics dependent. As a result, intuition about physics such as the role of short-range correlations or D-state mixing in particular kinematic regimes can be strongly scale dependent. Understanding this dependence is crucial in making use of extracted properties.

DOI: 10.1103/PhysRevC.96.054004

I. INTRODUCTION

Structure information about nuclei is often deduced from knock-out processes, such as $(p,2p)$ reactions or high-momentum electron scattering. Isolating the nuclear structure properties from the reaction dynamics in a *process-independent* manner requires a controlled factorization of structure and reaction. This factorization is always to some degree scale and scheme dependent, because the dividing point between structure and reaction is not unique. Understanding this dependence is important for robust extractions from experiment, to correctly use the structure information in other processes, and to understand the impact of approximations for both [1,2].

Scale and scheme dependence in quantum field theoretic treatments of knock-out reactions, such as high-energy scattering in quantum chromodynamics [3,4], is manifested in explicit factorization and renormalization prescriptions. In a nonrelativistic many-body treatment, scale and scheme dependence is hidden in the choice of internucleon potentials and associated currents. These approaches to knock-out processes are bridged by nuclear effective field theories (EFTs) [5–8], where the scale is associated with the value of a cutoff parameter and the scheme with the choice of regulator (and other details of renormalization).

We sometimes refer to this scale dependence as a resolution dependence [2,9], because the wavelengths available are restricted by the potential. It is important to distinguish this resolution implied by the potential from the experimental resolution, which is dictated by the kinematics of the experiment. The latter is fixed for a given experiment while the former can be changed continuously, e.g., by unitary transformations.

While the cross sections for knock-out reactions are independent of the factorization scale, the individual components of a theoretical calculation—initial state, interaction current, and final-state interactions (FSIs)—are not. As we show, for some kinematics the FSI contribution can be substantial at high resolution but largely absent at a lower resolution. Furthermore, the physics interpretation of the process can change with scale. What is dominantly short-range correlation and/or D-state structure physics at one scale can be mostly low-momentum S-state physics at another scale.

The changing interplay of the different components as the scale changes is often not immediately intuitive. For example, how do cross sections remain invariant as one-body currents become two-body currents and short-range structure disappears? The goal of this paper is to present a clean,

*more@nscl.msu.edu
†bogner@nscl.msu.edu
‡furnstahl.1@osu.edu

focused example that illustrates the interplay without getting lost in approximations, which opens the door to an intuitive understanding of scale-dependent features that we hope can one day be transferred to more complicated nuclear processes.

Ultimately a pertinent question is this: What is the best choice of scale? Some motivations for that choice include the following:

To make calculations easier or more convergent. In field theory, this can mean choosing the QCD running coupling and scale to improve perturbation theory. For many-body problems, this could mean using a soft potential to improve many-body convergence, or to make microscopic connections to the shell model or density functional theory [9].

Better interpretation or intuition, which can lead to more predictability. For example, short-range correlation (SRC) phenomenology for high-momentum-transfer electron scattering from nuclei has many successes in explaining and predicting experiment [10–13]. But, as we see, a low-resolution scale can also lead to an intuitive picture, with complementary advantages.

Allowing for the cleanest extraction from experiment. Final-state interactions are usually a hindrance to extracting structure information from electron scattering measurements. Can the choice of scale allow one to "optimize" the validity of the impulse approximation or the assumed factorization of structure and reaction? Ideally one extracts from a given experiment at the optimal scale for the kinematics, then relates to other scales to compare to other experimental or theoretical predictions. In inclusive high-energy QCD scattering, the optimal scale is typically the four-momentum transfer squared of the experiment, but this is not universally true [4].

To study scale dependence and relate nuclear processes at different scales, the renormalization group (RG) has proven to be a powerful method [14,15]. But conventional nuclear knock-out experiments have not been analyzed using variable resolution with RG methods. We strongly advocate embedding the usual approaches in an RG framework, which will provide interconnections between calculations with different potentials and with different approaches such as EFTs and use of the operator product expansion (OPE) [16,17]. The present work is a contribution toward realizing this framework.

A candidate RG framework for nuclear applications is the similarity renormalization group (SRG), which is a useful and versatile tool for such questions [9,14,18–26]. The SRG has been widely applied for nuclear structure applications, both to soften the internucleon potential in free space and as a many-body solution method in the form of the in-medium SRG [27]. The improved convergence has also enabled *ab initio* reaction calculations using the no-core shell model–resonating group method approach [28,29].

A recent paper [30] made the first SRG application to the simplest, cleanest knock-out reaction: deuteron electrodisintegration. This process provides an excellent laboratory for exploring issues of scale dependence. Reference [30] considered various kinematic regions of the longitudinal structure function f_L and showed how the different ingredients for calculating this observable—deuteron wave function, zeroth component of the electromagnetic current, and relative scattering wave function for the final proton and neutron—evolved under a change of scale. Each ingredient changed via an SRG unitary transformation in such a way to leave f_L unchanged. The qualitative nature of the changes varied strongly with the kinematics.

Here we revisit this process for kinematic regions that exhibit strong scale dependence of the ingredients and examine the components at different scales to understand better the physics behind the evolution. For high momentum transfers moderately close to threshold, we find that an intuitive high-resolution picture of the process in impulse approximation as a one-body current breaking up a short-range correlated neutron-proton pair is evolved to a different intuitive picture with simpler initial *and* final state wave functions and a simple two-body current. The latter combine to allow a simple calculation that is sensitive to different structure aspects than the high-resolution analysis. For example, sensitivity to the D-state component of the deuteron at high resolution becomes complete insensitivity at low resolution.

The plan of the paper is as follows. In Sec. II we recap details and results of Ref. [30], and review some relevant SRG formalism and results. We analyze deuteron electrodisintegration at different resolution scales for particular kinematics in Sec. III that show strong effects of evolution, including greatly reduced FSI, and demonstrate that the induced two-body current can be expanded efficiently. We finish in Sec. IV with a summary and illustration of how intuition such as the sensitivity to the D-state probability can change with scale.

II. BACKGROUND AND FORMALISM

A. Deuteron electrodisintegration formalism

The deuteron electrodisintegration process is an ideal testing ground for a robust analysis of knock-out reaction scale dependence because we are able to calculate all of the components accurately at different resolutions for a given approximation [30]. The $d(e,e'p)n$ reaction is the simplest knock-out process and is widely used for benchmarking nucleon-nucleon (NN) interactions [31]. The evolution of the current and wave functions is sufficiently rich for a first application of SRG methods to reactions, while the restriction to a two-body system postpones the complications of three-body forces and currents.

To further simplify our analysis, we focus on the longitudinal structure function f_L, which up to some kinematic factors is related to an experimental cross section and is therefore an RG-invariant observable. The longitudinal structure function is given by [30,31]

$$f_L(p',\theta',q) = \mathcal{C} \sum_{m_s,\, m_J} |\langle \psi_f(m_s,p',\theta')|J_0(q)|\psi_i(m_J)\rangle|^2, \quad (1)$$

where p' is the magnitude of three-momentum of the outgoing proton, θ' is the angle that the outgoing proton makes with the virtual photon axis (taken to be along $\hat{z}$), and q is the three-momentum transferred by the virtual photon. All these quantities are in the center-of-mass frame of the outgoing nucleons. ψ_f and ψ_i are the final scattering state wave function of the outgoing nucleons and the initial deuteron state wave function, respectively, with m_s and m_J the corresponding

quantum numbers. The constant $\mathcal{C}$ in Eq. (1) is a kinematic factor involving p, q, deuteron mass, and the nucleon mass [30].

The relevant one-body current matrix element is given by

$$\begin{aligned}\langle \mathbf{k}_1 T_1 | J_0(\mathbf{q}) | \mathbf{k}_2 T = 0 \rangle \\ = \tfrac{1}{2}\left(G_E^p + (-1)^{T_1} G_E^n\right)\delta(\mathbf{k}_1 - \mathbf{k}_2 - \mathbf{q}/2) \\ + \tfrac{1}{2}\left((-1)^{T_1} G_E^p + G_E^n\right)\delta(\mathbf{k}_1 - \mathbf{k}_2 + \mathbf{q}/2). \end{aligned} \quad (2)$$

Here G_E^p and G_E^n are the proton and neutron electric form factors. The deuteron state has isospin $T = 0$, and therefore the ket in Eq. (2) is restricted to $T = 0$. The final-state wave function of the outgoing proton-neutron pair with relative momentum p' is found from

$$|\psi_{f\,p'}\rangle = |\phi_{p'}\rangle + G_0(E')\,t(E')\,|\phi_{p'}\rangle, \quad (3)$$

where $|\phi_{p'}\rangle$ is a relative plane wave, G_0 and t are the Green's function and the t-matrix, respectively, with outgoing boundary conditions, and $E' = p'^2/M_{np}$ is the energy of outgoing nucleons. The impulse approximation (IA) is defined here by neglecting the interaction between the outgoing nucleons [given by the second term in Eq. (3)] and taking $|\psi_{f\,p'}\rangle_{\rm IA} \equiv |\phi_{p'}\rangle$. We call this the IA even when we have an induced two-body current.

We note that in our work the kinematic variables we use are E', the energy of outgoing nucleons; $\mathbf{q}^2_{\rm c.m.}$ (also denoted as q^2), the three-momentum transferred by the virtual photon; and θ', the angle that the outgoing proton makes with the photon. All these quantities are in the center-of-mass frame of the outgoing nucleons. Another set of kinematic variables that are used for electron scattering from nuclei are Bjorken x and the four-momentum Q^2. In Appendix A we relate x and Q^2 to E' and $\mathbf{q}^2_{\rm c.m.}$.

Our formalism implies a nonrelativistic treatment, but to ensure clear demonstrations of scale dependence we apply it for some kinematic regions where that might be questionable. However, we do so consistently at each resolution, so the comparison at different scales will always be valid, even though comparison to experiment will not be so useful or informative (also because we omit initial two-body currents).

B. Local decoupling with SRG

The SRG for nuclear applications is well documented in the literature [9,14,18,19,32] but we briefly summarize the salient points. The simplest SRG transformations are realized as a flow equation, which is a differential equation for the Hamiltonian that induces a continuous series of infinitesimal unitary transformations:

$$\frac{dH_s}{ds} = [[G_s, H_s], H_s], \quad (4)$$

where s is a flow parameter. Here, and in most nuclear applications to date, the operator G_s is the kinetic energy operator T and the flow equation becomes (with $V_s \equiv H_s - T$)

$$\frac{dV_s}{ds} = [[T, V_s], T] + [[T, V_s], V_s]. \quad (5)$$

We solve Eq. (5) in a partial-wave momentum basis, where it becomes a set of coupled differential equations for the matrix elements of the potential.

The SRG equations decouple high-energy from low-energy degrees of freedom in the Hamiltonian by driving far off-diagonal matrix elements to zero. (Other choices of G_s also achieve this goal with different decoupling patterns.) The degree of decoupling is characterized by the scale $\lambda = s^{\frac{1}{4}}$, which has units of momentum, and we use λ to characterize the flow in what follows and in our notation (so V_s becomes V_λ). The first term in Eq. (5) dominates far off-diagonal matrix elements; keeping this term only yields the solution for the NN potential (with mass $M = 1$):

$$V_\lambda(k,k') \approx V_{\lambda=\infty}(k,k') e^{-\left(\frac{k^2-k'^2}{\lambda^2}\right)^2}. \quad (6)$$

This shows that λ^2 is roughly the maximum difference between kinetic energies of nonzero matrix elements.

Figures 1 and 2 provide an intuitive picture of decoupling and the role of λ as a decoupling scale. Here $V_{\lambda=\infty}$ is the AV18 potential [33] and evolution is shown for two blocks of the ${}^3S_1$–${}^3D_1$ coupled channel. For convenience in comparing to momentum scales, we plot the potential using the relative momenta. This obscures somewhat the uniform decoupling in k^2 that is implied by Eq. (6); it is manifested for potentials plotted as functions of k^2, k'^2 (e.g., see Fig. 9 in Ref. [14]).

The partial diagonalization of V_λ leads to *local* decoupling [32]. This means that only matrix elements with relative

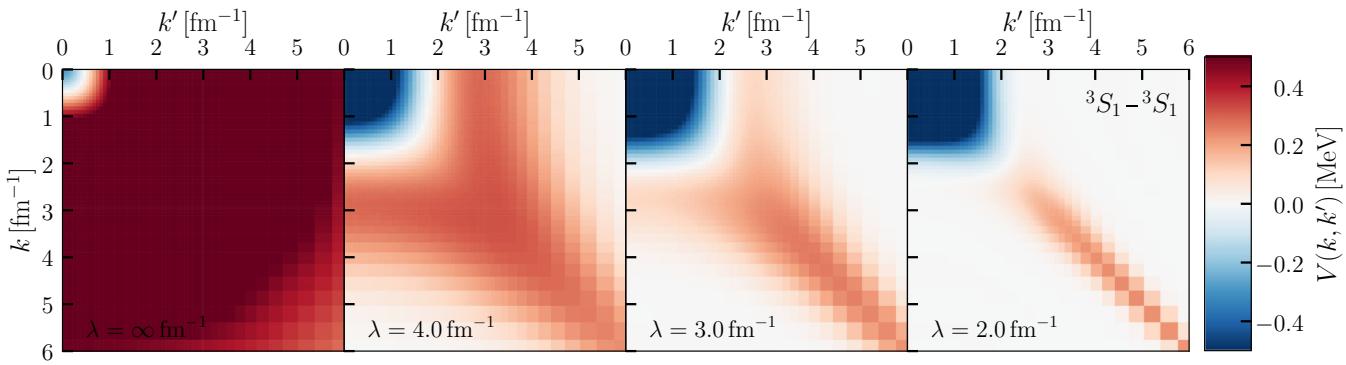

FIG. 1. SRG running of the AV18 potential in the ${}^3S_1$–${}^3S_1$ channel.

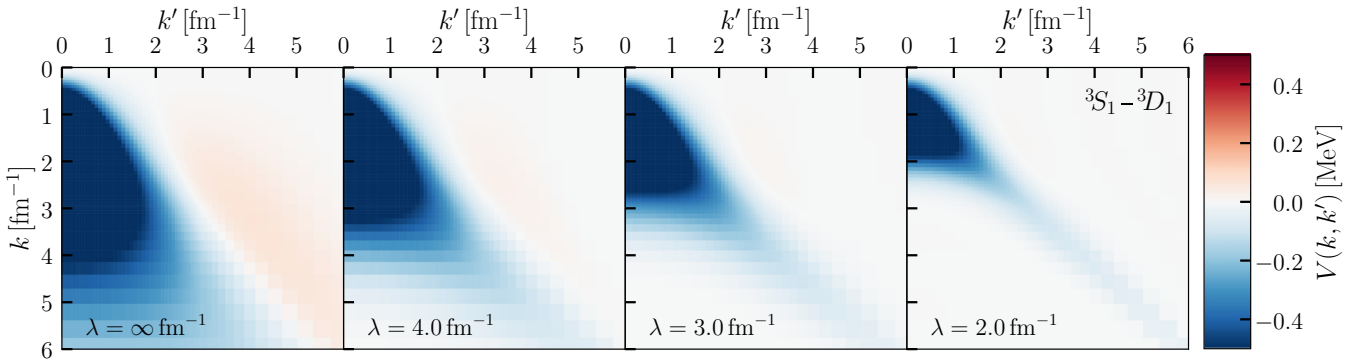

FIG. 2. SRG running of the AV18 potential in the $^3S_1$–$^3D_1$ channel.

momentum arguments differing by less than roughly λ contribute in the Lippmann-Schwinger equation for the t-matrix or wave functions. This in turn leads to a lower *resolution* as the potential evolves—local decoupling means that only wavelengths in a narrow region are available to build wave functions. We make the association of limited wavelengths and limited resolution (as with diffraction), although in past investigations we were typically restricted to low momentum only. Here we have the possibility of high-relative-momentum final states.

The impact that local decoupling of the potential has on the deuteron wave function is shown in Figs. 3 and 4, with complementary effects in position and momentum space. For the S-wave part, the high-momentum tail from the strong coupling of low and high momentum in the original AV18 potential ($\lambda = \infty$) is evolved away as λ is reduced, with a consequent filling in of the wound in the small-r part of the wave function. For the D-wave part, the D-state probability is steadily reduced, as implied by the reduced S-D tensor coupling in the potential. This reduction is clearly evident in position space, where the interior part of the D-state component of the wave function is greatly reduced in evolving from $\lambda = \infty$ to $\lambda = 2\,\text{fm}^{-1}$. Note that the position-space tails, which are specified by deuteron asymptotic normalization constants, are RG invariant, as expected because they are exterior quantities [34].

Because λ sets a separation scale in the deuteron, we identify the subsequent SRG evolution of the wave function as a change in scale. The change in the deuteron momentum distribution is analogous to the RG evolution of the parton distribution function for up or down quarks in the proton [2]. In the latter case there is also a clear *scheme* dependence, which refers to the prescriptions for renormalization and factorization (how the short- and long-distance parts are divided). The SRG evolution changes the scale but not the scheme because these are unitary transformations with a fixed SRG generator. The scheme dependence is instead in the choice of the initial NN potential and the choice of the generator.[1] The difference between scale and scheme dependence is manifested by different sets of chiral EFT potentials in the literature (e.g., Refs. [35–38]). The sets differ by scheme (e.g., the choice of regulator can be nonlocal, local, or semilocal) and within each set differ by scale (determined by the value of the regulator parameter). The guidance about schemes from the *Handbook*

[1]Note that the flow to universal potentials can eliminate the scheme dependence due to the initial potential if all momenta are less than λ.

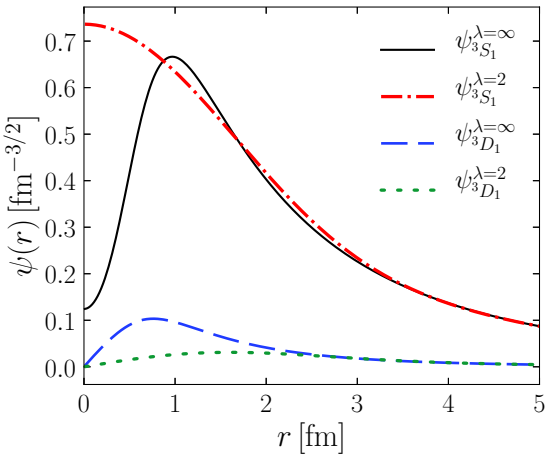

FIG. 3. Deuteron wave functions in position space for the unevolved ($\lambda = \infty$) and evolved (to $\lambda = 2\,\text{fm}^{-1}$) AV18 potential.

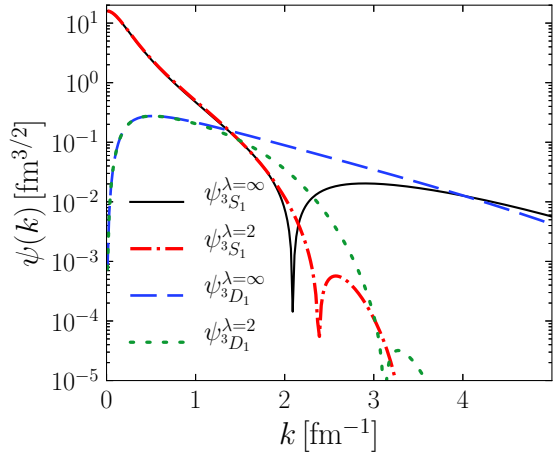

FIG. 4. Deuteron wave functions in momentum space for the unevolved ($\lambda = \infty$) and evolved (to $\lambda = 2\,\text{fm}^{-1}$) AV18 potential.

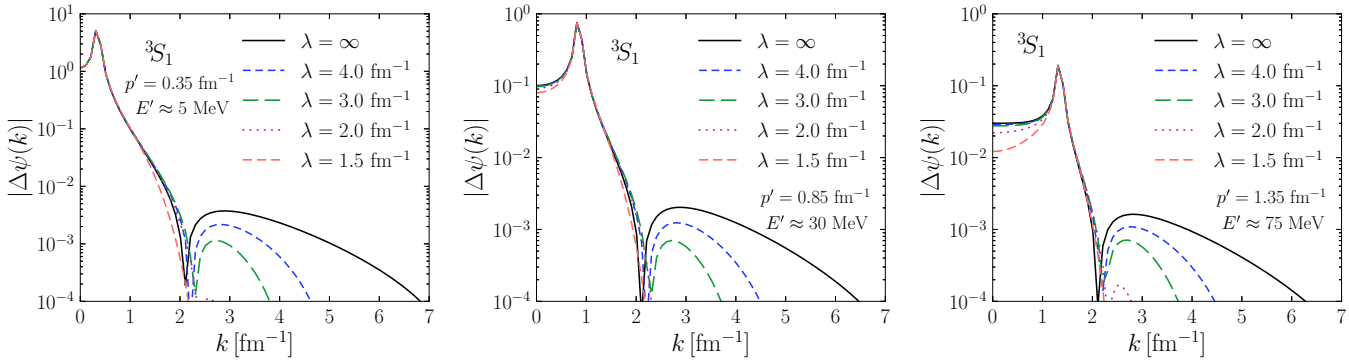

FIG. 5. $|\Delta\psi^\lambda(p';k)|$ in the $^3S_1$ channel for various p' and SRG λ values. $\Delta\psi^\lambda(p';k)$ in the evolved case is suppressed for large momentum. For large p', the values of $\Delta\psi^\lambda(p';k)$ even at small momenta differ for different SRG λs.

of Perturbative QCD applies equally to low-energy nuclear processes [3]:

> The choice of scheme is a matter of taste and convenience, but it is absolutely crucial to use schemes consistently, and to know in which scheme any given calculation, or comparison to data, is carried out.

In nuclear reaction applications, one must evolve all components—initial state, current, and final state—of the matrix elements for cross sections to remain invariant. This is conveniently carried out for deuteron electrodisintegration in terms of the integrated unitary transformation operator $\widehat{U}_\lambda$ [30]:

$$|\psi_\lambda\rangle = \widehat{U}_\lambda|\psi_{\lambda=\infty}\rangle, \quad \widehat{O}_\lambda = \widehat{U}_\lambda\widehat{O}_{\lambda=\infty}\widehat{U}_\lambda^\dagger, \tag{7}$$

where $|\psi_\lambda\rangle$ is an initial or final state and $\widehat{O}_\lambda$ is an operator such as the Hamiltonian or the interaction current. If the energy or momentum scale of the external probe is significantly larger than λ, then the scale separation with respect to the ground state wave function (which has only momenta less than roughly λ) leads to a factorization of matrix elements of the $\widehat{U}_\lambda$ [39]:

$$U_\lambda(k,q) \longrightarrow K_\lambda(k)Q_\lambda(q) \quad \text{when } k < \lambda \text{ and } q \gg \lambda. \tag{8}$$

In the next section we show how the change in the current induced by the unitary transformation can be efficiently expanded in factorized form with a singular value decomposition.

III. RESULTS

A. Scattering state evolution

We begin by analyzing how the scattering state $\psi^\lambda(p';k) \equiv \phi_{p'}(k) + \Delta\psi^\lambda(p';k)$ of the outgoing proton-neutron pair evolves under the SRG for different values of p' and λ. Multiplying Eq. (3) from the left by $\langle k|$ and projecting onto partial waves gives

$$\begin{aligned}&\langle k_1 J_1 m_{J_1} L_1 S_1 T_1|\phi_{p'}\rangle \\ &= \frac{1}{2}\sqrt{\frac{2}{\pi}}\frac{\pi}{2}\frac{\delta(p'-k_1)}{k_1^2}\langle J_1 m_{J_1}|L_1 m_{J_1} - m_{s_f}\, S_1 m_{s_f}\rangle \\ &\quad\times(1+(-1)^{T_1}(-1)^{L_1})Y^*_{L_1 m_{J_1}-m_{s_f}}(\theta',\varphi')\end{aligned} \tag{9}$$

for the free plane-wave, and

$$\begin{aligned}&\Delta\psi^\lambda(p';k) \\ &= \langle k\, J_1 m_{J_d}\, L_1\, S_1\, T_1|G_0^{E'}t^\lambda(E')|\phi(p',J_1,S_1,T_1,m_{s_f})\rangle \\ &= \frac{1}{2}\sqrt{\frac{2}{\pi}}\frac{1}{p'^2-k^2+i\epsilon}\sum_{L_2} t^\lambda(k,p',E',L_1,L_2,J_1,S_1,T_1) \\ &\quad\times\langle J_1 m_{J_d}|L_2 m_{J_d} - m_{s_f}\, S_1 m_{s_f}\rangle \\ &\quad\times(1+(-1)^{T_1}(-1)^{L_2})Y^*_{L_2 m_{J_d}-m_{s_f}}(\theta',\varphi')\end{aligned} \tag{10}$$

for the scattered wave that contains the effects of final-state interactions between the outgoing nucleons. Here and below, θ' and φ' are the angles of the outgoing proton with respect to the virtual photon. Note that $\Delta\psi^\lambda(p';k)$ is singular at the on-shell momentum $k = p'$, and is in general complex valued.

In Fig. 5 we plot the magnitude of $\Delta\psi^\lambda(p';k)$ (omitting the singular point $k = p'$) in the $^3S_1$ channel for various p' and λ values. As expected from SRG decoupling, $\Delta\psi^\lambda(p';k)$ in the evolved case becomes suppressed for large momentum $k \gtrsim \lambda$. As p' increases, the values of $\Delta\psi^\lambda(p';k)$ at small momenta are also suppressed with decreasing SRG λs. This reflects the local decoupling with SRG evolution for large p'; the wave function is suppressed for momenta more than λ from p' in either direction [32].

It is instructive to also look at the scattering wave function in coordinate space, using

$$\psi^\lambda(p';r) = \int \mathrm{d}k\, k^2\, j_l(k\,r)\psi^\lambda(p';k). \tag{11}$$

Figure 6 shows $|\psi^\lambda(p';r)|$ in the $^3S_1$ channel for different p' and SRG λs. As expected, $\psi^\infty(r)$ has a sizable correlation wound at short distances (up to about 1 fm) that is progressively filled in as the wave functions evolve to lower λ values. Note that beyond the range of the potential, $\psi(r)$ and $\phi(r)$ differ as expected by just a phase that is the same for all values of λ.

B. Operator evolution

The operator of interest here is the deuteron disintegration current operator, which is just the zeroth component of the electromagnetic current. The matrix element of the one-body current operator used in Ref. [30] is given by Eq. (2).

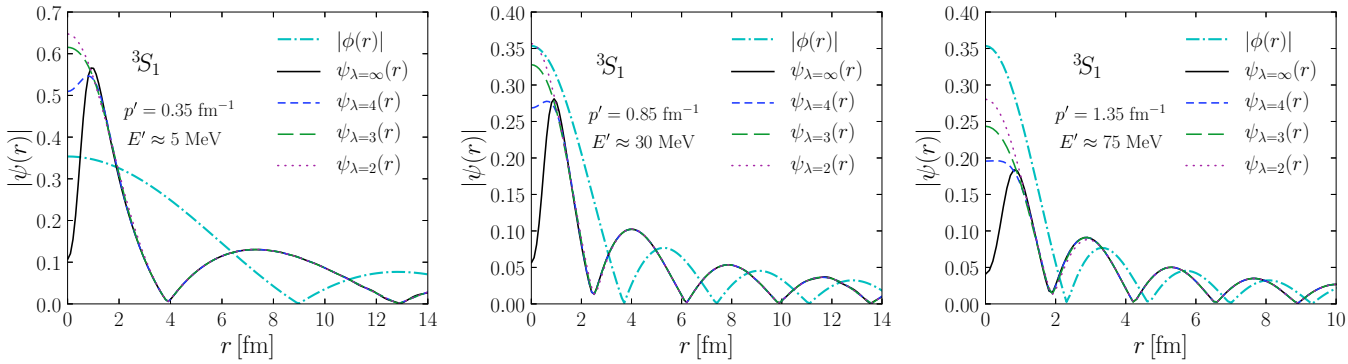

FIG. 6. $|\psi^{\lambda}(p';r)|$ in the $^3S_1$ channel for various p' and SRG λ values. $\psi^{\infty}(r)$ has a correlation wound at short distances that is absent for the evolved wave functions.

We denote the first term in Eq. (2) by J_0^-. In the following we focus only on results obtained from using J_0^-, as it was verified in Ref. [30] that $\langle\psi_f|J_0|\psi_i\rangle = 2\langle\psi_f|J_0^-|\psi_i\rangle$. In the partial-wave basis, the J_0^- matrix element is given by

$$\begin{aligned}\langle k_1 J_1 m_{J_d} L_1 S = 1, \quad T_1|J_0^-|k_2 J = 1\, m_{J_d}\, L_2\, S = 1\, T = 0\rangle \\ = \frac{\pi^2}{2}\left(G_E^p + (-1)^{T_1} G_E^n\right) \\ \times \sum_{\widetilde{m}_s=-1}^{1} \left\langle J_1\, m_{J_d}\middle| L_1\, m_{J_d} - \widetilde{m}_s\; S = 1\, \widetilde{m}_s\right\rangle \\ \times P_{L_1}^{m_{J_d}-\widetilde{m}_s}\left(\frac{k_1^2 - k_2^2 + q^2/4}{k_1 q}\right)\frac{2}{k_1 k_2 q} \\ \times P_{L_2}^{m_{J_d}-\widetilde{m}_s}\left(\frac{k_1^2 - k_2^2 - q^2/4}{k_2 q}\right) \\ \times \left\langle L_2 m_{J_d} - \widetilde{m}_s S = 1 \widetilde{m}_s J = 1 m_{J_d}\right\rangle \qquad (12)\end{aligned}$$

when

$$k_2 \in (|k_1 - q/2|, k_1 + q/2) \qquad (13)$$

and equals zero otherwise.

In Figs. 7 and 8 we show heat map plots of $J_0^{\lambda} \equiv U_{\lambda} J_0^{\infty} U_{\lambda}^{\dagger}$ for $q = 6\,\mathrm{fm}^{-1}$ in the partial wave basis, which are representative of the characteristics of the current under SRG evolution. The unevolved current is a one-body operator and is peaked at $(0,q/2)$ and $(q/2,0)$. Under SRG evolution with $G_s = T$, the one-body part is unchanged but the current develops two-body components, ΔJ_0^{λ}. As seen in Figs. 7 and 8, the changes due to evolution are smooth and distributed for momenta less than $q/2$, and the evolved current does not become pathologically large at high momentum. This is important because for practical calculations the evolved current will be used in conjunction with the evolved wave functions. These wave functions have negligible strength at high momentum and the absence of pathologies in the evolved current make calculations with the SRG in a reduced basis possible [39].

C. Final-state interactions

Final-state interactions often complicate the extraction of structure information from electron scattering measurements. Having shown that the individual ingredients of the observable cross section are by definition scale- and scheme-dependent quantities, it is interesting to ask if one can choose the resolution scale to minimize the importance of FSIs in certain kinematics. We use the case of large p' as an example, taking $p' = 1.5\,\mathrm{fm}^{-1}$ and considering λ values both larger and smaller than p'. Recall from Eq. (3) that the scattering wave function is given by the sum of a free plane wave and the modification

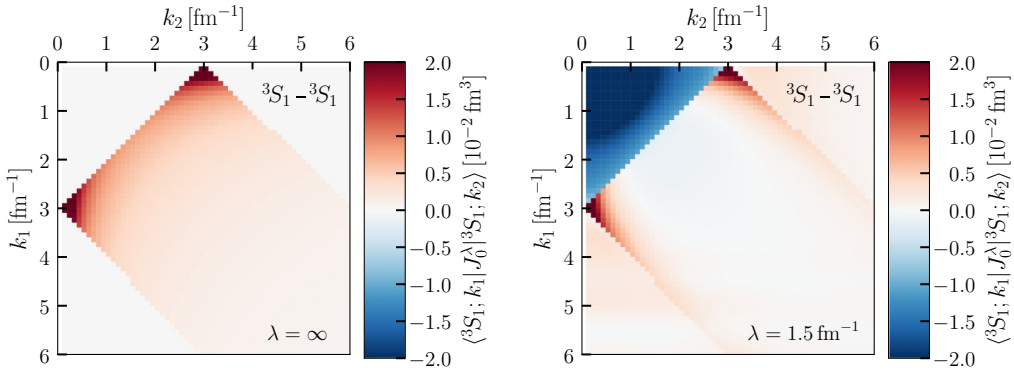

FIG. 7. Heat map plot for the unevolved ($\lambda = \infty$) and the evolved current ($\lambda = 1.5\,\mathrm{fm}^{-1}$) for $q^2 = 36\,\mathrm{fm}^{-2}$ in the $^3S_1$–$^3S_1$ block for $m_{J_d} = 0$. The heat map plots for $m_{J_d} = 1$ look very similar. The unevolved current is peaked at $(0,q/2)$ and $(q/2,0)$. SRG evolution induces smooth two-body currents in the low-momentum region.

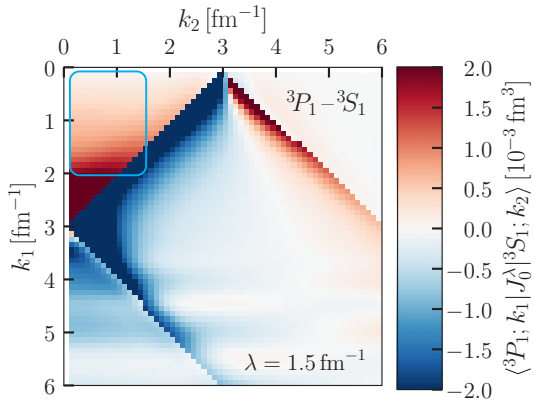

FIG. 8. Heat map plot for the evolved current ($\lambda = 1.5\,\mathrm{fm}^{-1}$) for $q^2 = 36\,\mathrm{fm}^{-2}$ in the ${}^3P_1$–${}^3S_1$ channel for $m_{J_d} = 1$. While the changes due to evolution are distributed, only the low-momentum region of the evolved current is relevant for our examples (see the boxed region). In this region, the evolved current is smooth and linear in k_1 [cf. Eq. (15)].

$\Delta\psi(k)$ due to the potential. The evolution of $|\Delta\psi(k)|$ is shown in Fig. 9, where we see a common peak near the on-shell point $k = p'$, but very different contributions at large and small k as a function of λ. For $p' \gtrsim \lambda$, $\Delta\psi(k)$ is well localized around $k = p'$ due to the local decoupling properties of the SRG with the present choice of generator.

In Figs. 10–13, we scan through a range of q^2 and show f_L for $\lambda = \infty$, 1.5, and 1.2 fm^{-1}. The efficacy of the IA for the unevolved ($\lambda = \infty$) calculations is highly dependent on q^2. At the large q^2 values shown in Figs. 10 and 11, which fall in the kinematic range commonly used to probe short-range correlations in nuclei [12,13], explicit calculations show that in the unevolved case, the high-momentum tail in the final-state wave function gives a sizable contribution to f_L, roughly a 100% correction at $q^2 = 49\,\mathrm{fm}^{-2}$. As q^2 is lowered, the correction decreases and for quasifree kinematics (here with $q^2 = 10\,\mathrm{fm}^{-2}$), there is only a small contribution from the FSI, as expected [40]. With a further lowering of the momentum transfer to $q^2 = 1\,\mathrm{fm}^{-2}$, the FSI correction is again very large.

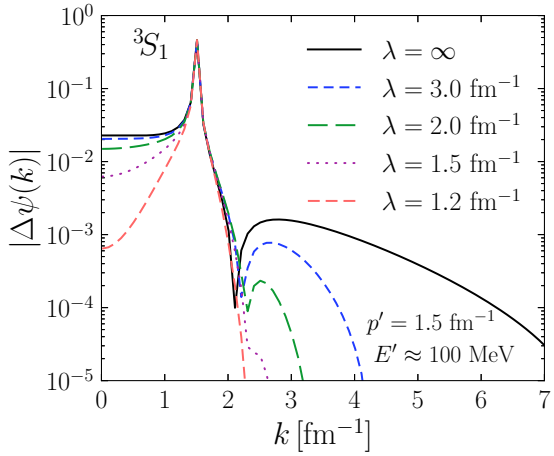

FIG. 9. Local decoupling in the final state of the ${}^3S_1$ partial wave at large momentum $p' = 1.5$ fm.

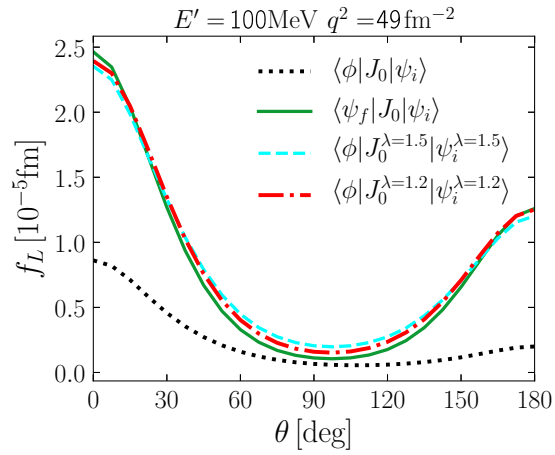

FIG. 10. Comparing the unevolved IA and the full calculations of f_L at $p' = 1.5\,\mathrm{fm}^{-1}$ (or $E' = 100$ MeV) and $q^2 = 49\,\mathrm{fm}^{-2}$ with the evolved IA result at $\lambda = 1.5\,\mathrm{fm}^{-1}$ and $\lambda = 1.2\,\mathrm{fm}^{-1}$. We find that the contribution of FSI is minimal in the evolved picture at this kinematics corresponding to $x_d = 1.64$ and $Q^2 = 1.78\,\mathrm{GeV}^2$.

In strong contrast, as we scan through the range of q^2, the IA answer in the *evolved* picture closely tracks the full FSI answer. This can be qualitatively understood from the contour plots of J_0^λ in Figs. 7 and 8, in conjunction with Figs. 4 and 9. Consider the two cases shown in Figs. 10 and 11 where $p' \sim \lambda < q/2$. The evolved deuteron wave function restricts the contribution from $J_0^\lambda(k,k')$ (cf. Fig. 7) to $k' \lesssim \lambda$, while the evolved final state primarily picks up contributions from $J_0^\lambda(k,k')$ for $k \approx p'$. For $p' < q/2$, this is the region where J_0^λ is smooth and well approximated by simple derivative and low-rank singular value decomposition (SVD) expansions (see Secs. III D and III E). Because $\Delta\psi_{p'}(k)$ is localized about $k \approx p'$, the final-state interaction is proportional to the on-shell t-matrix, which is small at large momentum.

As we decrease q, we approach the quasifree ridge (cf. Fig. 12) characterized by $p' \approx q/2$ (also note that $x_d \approx 1$). Note from Fig. 7 that most of the strength of J_0^λ is concentrated around $p' \approx q/2$. This is the region where the FSI contributions are small regardless of the choice of the SRG scale [30].

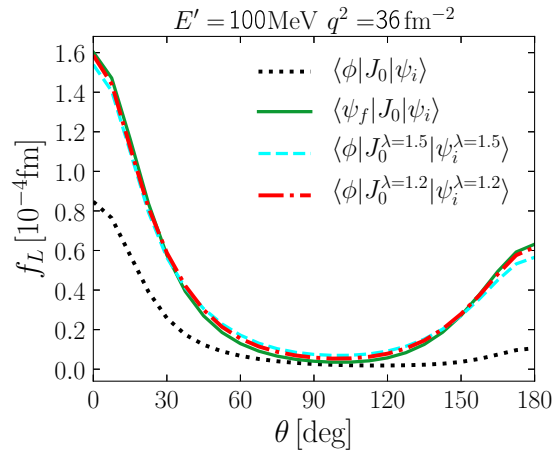

FIG. 11. Same as Fig. 10 but at $q^2 = 36\,\mathrm{fm}^{-2}$. Here $x_d = 1.55$ and $Q^2 = 1.34\,\mathrm{GeV}^2$.

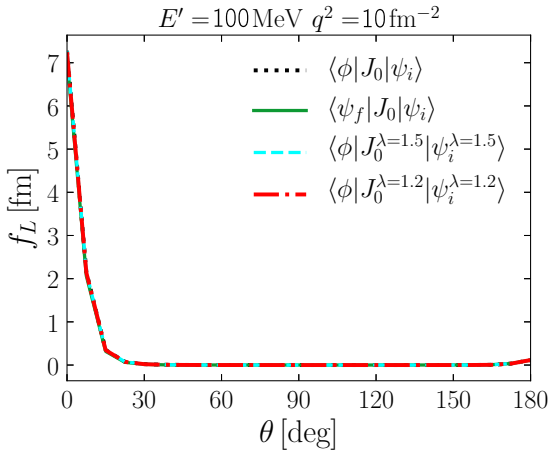

FIG. 12. Comparing the unevolved IA and the full calculations of f_L at $E' = 100$ MeV and $q^2 = 10\,\mathrm{fm}^{-2}$ with the evolved IA result at $\lambda = 1.5\,\mathrm{fm}^{-1}$ and $\lambda = 1.2\,\mathrm{fm}^{-1}$. This kinematics with $x_d = 0.99$ and $Q^2 = 0.39\,\mathrm{GeV}^2$ corresponds to the quasifree ridge. At the quasifree ridge, the contributions from the FSI are small for all SRG scales.

As we decrease q even further, we are in the region where $p' > q/2$. Here ψ_f^λ picks contributions from $J_0^\lambda(k,k')$ in the region $k > q/2$. Unlike the $k < q/2$ region, the form of J_0^λ at large momentum is not smooth in momentum (cf. Fig. 8) and therefore little can be said about the effect of evolution on the IA. Moreover, as seen from the x_d and Q^2 values, unlike the kinematics in Figs. 10 and 11, the kinematics in Fig. 13 is not of much experimental interest.

D. Derivative expansion at low resolution

Conventional wisdom holds that simple low-resolution wave functions inevitably lead to complicated reaction calculations (and interpretations) because the relevant transition operators are transformed to more complicated forms. One might expect these complications to be especially severe for operators that probe the high-momentum structure of nuclear wave functions, such as the current operator $J_0(\mathbf{q})$ at large q^2, since such components are highly suppressed or completely absent from low-resolution wave functions [13]. However, in this regime new simplifications emerge due to the separation of scales $\lambda \ll q$, with the induced terms taking the form of an EFT derivative expansion, where each term consists of a λ-dependent coupling constant that encodes the effects of decoupled high-momentum states, multiplied by a regulated contact interaction that is the same for all operators with the same symmetries [41].

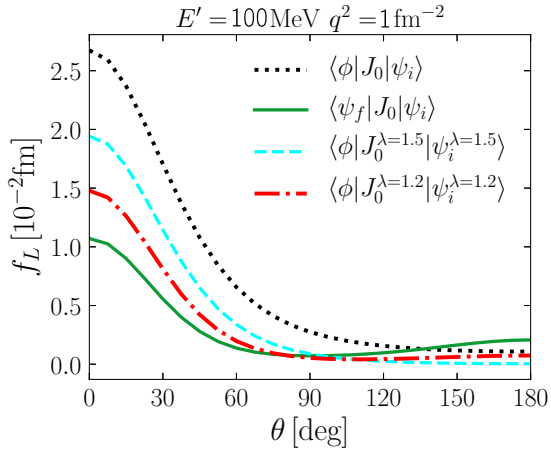

FIG. 13. Comparing the unevolved IA and the full calculations of f_L at $p' = 1.5\,\mathrm{fm}^{-1}$ (or $E' = 100$ MeV) and $q^2 = 1\,\mathrm{fm}^{-2}$ with the evolved IA result at $\lambda = 1.5\,\mathrm{fm}^{-1}$ and $\lambda = 1.2\,\mathrm{fm}^{-1}$. In the region $p' > q/2$, ψ_f^λ picks the contribution from the nonsmooth high-momentum region of $J_0^\lambda(k,k')$. Here $x_d = 0.14$, $Q^2 = 0.03\,\mathrm{GeV}^2$.

In the case of deuteron electrodisintegration for $p < \lambda \ll q/2$, the initial- and final-state wave functions predominantly probe the low-momentum components of the evolved current $J_0^\lambda(q)$. Because the one-body component of the current does not evolve under the SRG and is sharply peaked at $(k,k') = (0,q/2)$ and $(q/2,0)$, the transition matrix element is only sensitive to the induced two-body current ΔJ_0^λ. The low-momentum part of ΔJ_0^λ can be expanded as

$$\langle {}^3S_1;k_1|\Delta J_0^\lambda(q)|{}^3S_1;k_2\rangle = g_0^{m_J}(q) + g_2^{m_J}(q)\big(k_1^2 + k_2^2\big) + \cdots, \tag{14}$$

$$\langle {}^3P_1;k_1|\Delta J_0^\lambda(q)|{}^3S_1;k_2\rangle = g_1^{m_J}(q)\,k_1 + g_3^{m_J}(q)\,k_1\,k_2^2 + \cdots, \tag{15}$$

and similarly for higher partial waves. The "low-energy constants" (LECs) $g_0^{m_J}, g_2^{m_J}$, etc., are in principle calculable as described in Ref. [41], although in the present work we extract them simply by fitting to the exact $\Delta J_0^\lambda(k',k;q)$ in each channel.

As a proof of principle, we calculate f_L at $\lambda = 1.5\,\mathrm{fm}^{-1}$ using the derivative expansion for ΔJ_0^λ at kinematics ($E' = 20\,\mathrm{MeV}$, $q^2 = 36\,\mathrm{fm}^{-2}$ or $x_d = 1.88$, $Q^2 = 1.3\,\mathrm{GeV}^2$) that are sensitive to short-range correlations at high resolution scales. Here, we only include the S state component of the deuteron wave function in the evolved picture. As we see in Sec. IV, this is a very good approximation for small p' and large q^2, i.e., $\langle\psi_f^\lambda|J_0^\lambda(q)|\psi_i^\lambda\rangle \approx \langle\psi_f^\lambda|J_0^\lambda(q)|\psi_i^{\lambda\,{}^3S_1}\rangle$.

Evaluation of the matrix element $\langle\psi_f^\lambda|J_0^\lambda(q)|\psi_i^{\lambda\,{}^3S_1}\rangle$ involves sums over partial wave channels for the final state, i.e.,

$$\begin{aligned}\big\langle\psi_f^\lambda\big|J_0^\lambda\big|\psi_i^{\lambda\,{}^3S_1}\big\rangle &= \big\langle\psi_f^\lambda\big|{}^3S_1\big\rangle \underbrace{\langle {}^3S_1|\Delta J_0^\lambda|{}^3S_1\rangle}_{\text{use der. exp.}} \big\langle {}^3S_1\big|\psi_i^{\lambda\,{}^3S_1}\big\rangle \\ &+ \sum_{J=0,1,2} \big\langle\psi_f^\lambda\big|{}^3P_J\big\rangle \underbrace{\langle {}^3P_J|\Delta J_0^\lambda|{}^3S_1\rangle}_{\text{use der. exp.}} \\ &\times \big\langle {}^3S_1\big|\psi_i^{\lambda\,{}^3S_1}\big\rangle \\ &+ \sum_{J=1,2,3} \big\langle\psi_f^\lambda\big|{}^3D_J\big\rangle \underbrace{\langle {}^3D_J|\Delta J_0^\lambda|{}^3S_1\rangle}_{\text{use der. exp.}} \\ &\times \big\langle {}^3S_1\big|\psi_i^{\lambda\,{}^3S_1}\big\rangle + \cdots,\end{aligned} \tag{16}$$

where we used that the contribution of the one-body part of the current is exponentially suppressed at these kinematics for

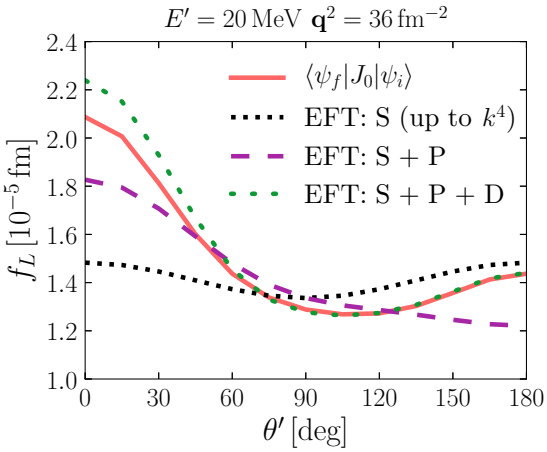

FIG. 14. Exact f_L (solid line) for $E_{np} = 20$ MeV and $q^2 = 36\,\mathrm{fm}^{-2}$ compared to f_L obtained using the derivative expansion for the evolved current ($\lambda = 1.5\,\mathrm{fm}^{-1}$). For this kinematics $x_d = 1.88$, $Q^2 = 1.3\,\mathrm{GeV}^2$.

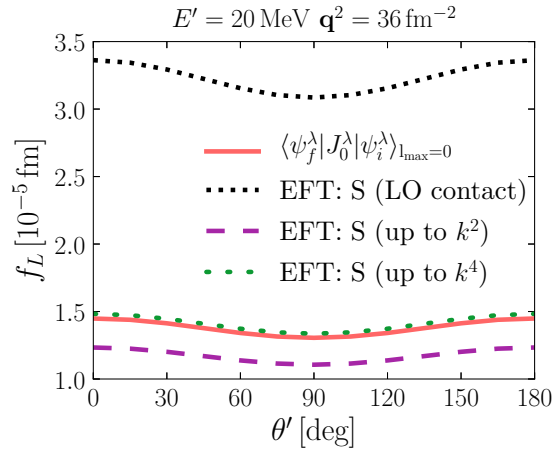

FIG. 15. Convergence of the derivative expansion in the S channel. Here $x_d = 1.88$, $Q^2 = 1.3\,\mathrm{GeV}^2$, and $\lambda = 1.5\,\mathrm{fm}^{-1}$.

small λ values. For the matrix elements of the evolved current in the given partial wave channel, we use the derivative expansion for that channel as in Eqs. (14) and (15).

Figure 14 shows results for f_L calculated using the derivative expansion as outlined above. The solid line in Fig. 14 is f_L calculated in the unevolved picture. The sparsely dotted line is f_L calculated keeping just the S channel in the final state [just the first term on the right-hand side of Eq. (16)], and for the derivative expansion of the evolved current we keep up to terms proportional to k^4 in Eq. (14). The dashed line is f_L calculated by including the S and P channel terms in the final state. In the derivative expansion for the P channel, we keep only the leading-order (LO) linear term in momentum in Eq. (15). Finally, the densely dotted line includes the correction to f_L from the D channel in the final state as well. Again, we only include the leading-order quadratic corrections in the derivative expansion for the evolved current in the D channel.[2] We find that f_L calculated in the low-resolution picture through the derivative expansion agrees very well with the unevolved answer. The agreement can be made even better by going to higher-order terms in the derivative expansion.

Note that in Fig. 14 we have added the next-to-next-to-leading-order (N2LO) correction for the S channel to the LO correction for the P and D channels. We find that keeping only the LO correction for the S channel gives a poor result. We illustrate this in Fig. 15.

The solid line in Fig. 15 corresponds to f_L calculated from the exact evolved current, but keeping only the S channels for the initial and final states. That is, f_L is calculated from the matrix element $\langle\psi_f^\lambda;{}^3S_1|J^\lambda_{0\,\mathrm{exact}}|\psi_i^\lambda;{}^3S_1\rangle$. This is then compared to f_L calculated from the derivative expansion for $\langle{}^3S_1;k_1|J^\lambda_{0\,\mathrm{exact}}|{}^3S_1;k_2\rangle$ going to successively higher terms in Eq. (14). We find that the LO answer from the derivative expansion misses the exact answer by about a factor of 2, but it gets rapidly better when we include higher-order terms in k^2.

E. SVD expansion at low resolution

A low-order derivative expansion of $\Delta J_0^\lambda(k',k)$ is most effective when the low-momentum components $k,k' \ll \lambda$ give the dominant contributions to the transition matrix element. However, for the f_L calculations, the integrals over the initial- and final-state wave functions do not saturate until $k,k' \approx 1.6\lambda$. In this sense, it is not surprising that the LO result in the S channel is rather poor.

A better way to arrange the expansion is suggested by the observation in Eq. (8) that the SRG transformation approximately factorizes, $U_\lambda(k,q) \approx K_\lambda(k)Q_\lambda(q)$, for well-separated momenta $k < \lambda \ll q$ [39]. Since it is precisely this portion of the U_λ matrix, plus the smooth low-momentum block $U_\lambda(k,k')$, that enters into the construction of the evolved current operator for the present kinematics, one expects that a low-rank SVD should efficiently capture the behavior of $\Delta J_q^\lambda \equiv \Delta J_0^\lambda(q)$. That is,

$$\langle k';{}^3L_J|\Delta J_q^\lambda|k;{}^3S_1\rangle \xrightarrow{\mathrm{SVD}} \sum_i c^q_{(i)}\, j^{(i)}_{\mathrm{left}}(k')\, j^{(i)}_{\mathrm{right}}(k), \qquad (17)$$

where $c^q_{(i)}$ are the singular values, and $j^{(i)}_{\mathrm{left}}$ and $j^{(i)}_{\mathrm{right}}$ are the left and right singular vectors, respectively, for the channel under consideration. As in Sec. III D, we keep only the ${}^3S_1$ channel in the deuteron evolved state and therefore ${}^3S_1$ in the ket in Eq. (17) in the current work. Extending to include the ${}^3D_1$ channel is straightforward.

The SVD analysis proceeds by constructing a matrix $\Delta J_q^\lambda(k_i,k_j)$ for $0 < k_i,k_j < k_{\max}$ for the given partial wave channel and performing the SVD to get the singular values and singular vectors. In the present work we choose $k_{\max} = 1.6\lambda$, which gives a truncation error from the integrals over the initial- and final-state wave functions of less than 0.5%. For the dominant $m_J = 0$ channels, we find that the first singular value is substantially larger than all the subsequent ones. For

[2]We find that the values for the $\langle{}^3D_1;k_1|\Delta J|{}^3S_1;k_2\rangle$ channel are not quadratic in k_1^2; however, they are about an order of magnitude smaller than the $\langle{}^3D_3;k_1|\Delta J|{}^3S_1;k_2\rangle$ channel. The smallness makes the ${}^3D_1$ channel inconsequential and we neglect it here.

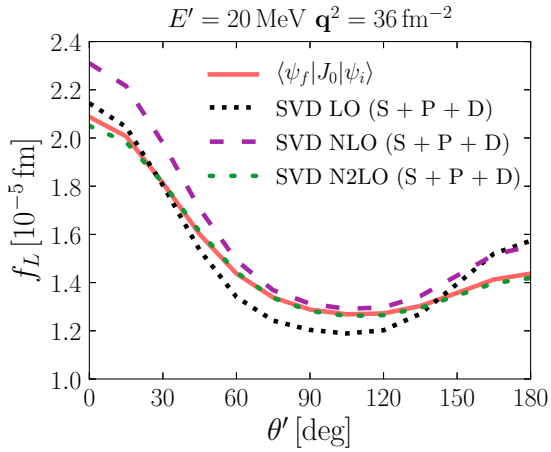

FIG. 16. Exact f_L (solid line) compared to f_L obtained using the SVD expansion for the evolved current at successive orders for $\lambda = 1.5\,\mathrm{fm}^{-1}$ and $k_{\max} = 1.6\lambda$. S+P+D indicates that we have gone up to the D channel in the partial wave expansion of the final state.

the subdominant $m_J = \pm 1$ channels, the first two singular values are of the same order of magnitude, with a substantial falloff thereafter. Once we have the singular values and vectors, we can put them together to get the transition matrix elements and ultimately f_L.

Figure 16 compares the exact f_L for the same kinematics as in Sec. III D to the f_L calculated using the SVD expansion for the evolved current. The LO result in Fig. 16 corresponds to keeping the first term in Eq. (17) for each channel, the next-to-leading-order (NLO) result corresponds to keeping the first two terms for each channel, and so on. Not surprisingly, given the smooth nature of the evolved current, we find that the SVD expansion quickly converges to the exact answer. We also find that the LO SVD is far superior to the LO derivative expansion. As shown in Fig. 17, in the S channel, the LO SVD agrees to within 10% of the exact result, while the LO derivative expansion is off by a factor of 2 (cf. Fig. 15). We speculate that this dramatic improvement can

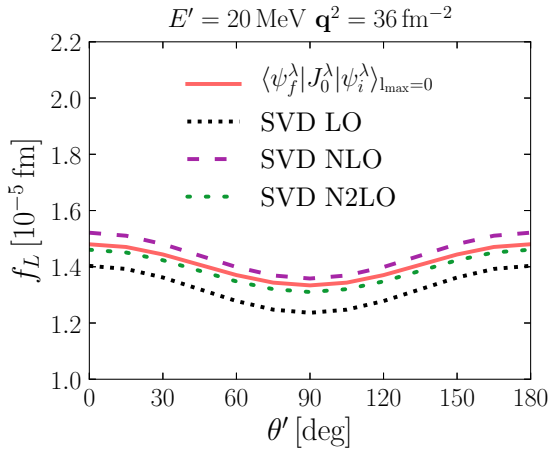

FIG. 17. Convergence of the SVD expansion in the S channel for $\lambda = 1.5\,\mathrm{fm}^{-1}$ and $k_{\max} = 1.6\lambda$. Here $x_d = 1.88$, $Q^2 = 1.3\,\mathrm{GeV}^2$.

TABLE I. Ratio of LO SVD matrix elements $\Delta J_q^\lambda(k_1,k_2)$ for two different q values at fixed $k_1 = 0.3\,\mathrm{fm}^{-1}$ and $k_2 = 0.5\,\mathrm{fm}^{-1}$, compared to the ratio of the corresponding LO singular values. The similar values in the two columns demonstrate that the q -dependence of $\Delta J(k_1,k_2)$ is mostly factorized in the singular values. Here $q_1^2 = 36\,\mathrm{fm}^{-2}$, $q_2^2 = 49\,\mathrm{fm}^{-2}$, and $\lambda = 1.5\,\mathrm{fm}^{-1}$.

	$\Delta J_{q_1}^{\lambda\,\mathrm{SVD\,LO}}/\Delta J_{q_2}^{\lambda\,\mathrm{SVD\,LO}}$	$c_{(1)}^{q_1}/c_{(1)}^{q_2}$
${}^3S_1$–${}^3S_1$ ($m_J = 0$)	2.099	1.89
${}^3P_1$–${}^3S_1$ ($m_J = 1$)	3.009	2.98

be understood as follows. The derivative expansion is an expansion in unregulated contact interactions,[3] whereas the low-momentum part of ΔJ_q^λ is smooth and takes the form of a *regulated* derivative expansion. The LO SVD is, therefore, analogous to a regulated contact interaction, with λ setting the scale of the regulator. Moreover, SVD through the shape of the singular vectors captures more of the actual physics of the system compared to imposing a regulator with arbitrary shape.

F. Factorization of q dependence

The derivative expansion for RG-evolved operators naturally factorizes the low- and high-momentum scales in a problem and gives a natural explanation for why certain quantities in many-body systems (e.g., high-momentum tails of momentum distributions and structure factors) scale off the corresponding quantities in few-body systems [41]. This separation is reflected in Eq. (15), where the q dependence of the evolved current operator is factorized into the LECs. We would like to check if an analogous separation holds for the SVD expansion of $\Delta J_q^\lambda(k',k)$, in which case we expect the majority of the q dependence is carried by the singular values.

To check this, we look at the ratio of the LO SVD expansion $\Delta J_q^\lambda(k',k)$ at small k for two different values of q ($q^2 = 36$ and $49\,\mathrm{fm}^{-2}$) and compare it to the ratios of the corresponding LO singular values. Referring to Table I, we see that most of the q dependence is indeed carried by the singular values. Another way to demonstrate the factorized q dependence is to look at the singular vectors. We do this in Fig. 18, where we find that the singular vectors for $q^2 = 36\,\mathrm{fm}^{-2}$ and $q^2 = 49\,\mathrm{fm}^{-2}$ are almost the same, indicating again that the dominant q dependence is carried by the singular values.

Armed with our knowledge of the factorized q dependence in the low-resolution picture, the interpretation of certain observations becomes quite straightforward. For instance, it is found that for small outgoing nucleon momentum (p') and large momentum transfer (q), the longitudinal structure function f_L factorizes into a function of p' and a function of q. This is demonstrated in Fig. 19. The plateau in the ratio of

[3]There are no ultraviolet divergences because the current is sandwiched between SRG-evolved wave functions, which only have support at low momentum.

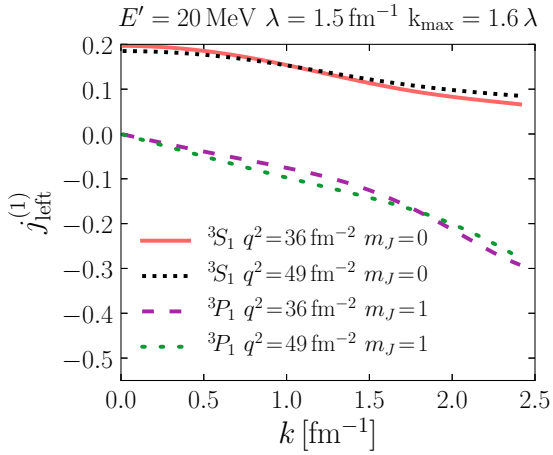

FIG. 18. Comparison of singular vectors for different q^2 for two different channels for $\lambda = 1.5\,\mathrm{fm}^{-1}$ and $k_{\mathrm{max}} = 1.6\lambda$.

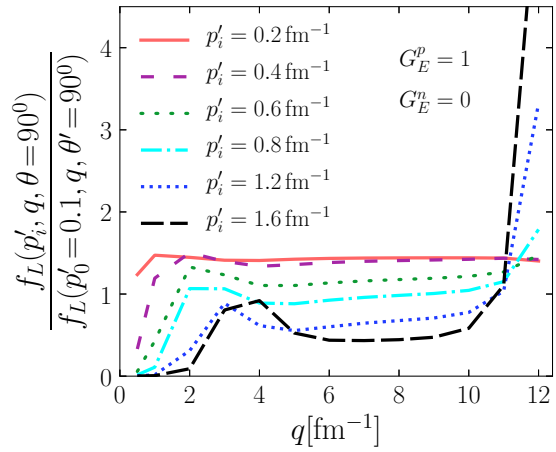

FIG. 19. Demonstration that for $p' \ll q$ the q dependence of f_L factorizes.

f_L shown in Fig. 19 tells us that, for $p' \ll q$,

$$f_L(p',\theta';q) \to g(p',\theta')B(q). \tag{18}$$

Here θ' is the proton emission angle.

Note that, as seen in Fig. 20, f_L by itself is a strong function of q. In the region where the ratio in Fig. 19 plateaus, the denominator of the ratio varies by over three orders of magnitude. Note that for simplicity we set the electric form factors for the proton and neutron to 1 and 0, respectively.

The explanation of factorization in Eq. (18) is straightforward in the low-resolution picture through the above SVD analysis. As we have seen, the LO term in Eq. (17) already gives a reasonable estimate in most cases. Moreover, from Table I, we find that most of the q dependence is carried by the leading singular value, so that the p' and q dependence is approximately factorized.[4] The factorization in the transition matrix element follows immediately and explains the plateaus in the ratios of f_L observed in Fig. 19.

Note that the factorization in Eq. (18) is the most prominent for $\theta' = 90^\circ$ and low p', because this is the region where the contribution from higher partial waves is minimal. For other angles and moderately large p' the matrix element $\langle\psi_f^\lambda|J_0^\lambda|\psi_i^\lambda\rangle$ will be a sum of factorized terms and therefore the q dependence of f_L will not necessarily factor out.

We would like to note that the preliminary analysis shows that the SVD works for higher energies as well as long as $p' < q/2$ (for instance the kinematics shown in Figs. 10 and 11). However, in order to compare the SVD answer to the exact answer, one needs to perform the SVD in more partial wave channels (than that shown in Fig. 16, for example) and in particular include the D state of the deuteron.

[4]The singular values weakly depend on p' if we use the physical values for the form factors instead of setting them to 1 and 0. This is because the form factors multiplying the current are a function of Q^2 [cf. Eq. (12)].

IV. SUMMARY AND OUTLOOK

In this work, we extended our use of deuteron electrodisintegration as a laboratory for exploring the consequences of scale dependence in nuclear knock-out reactions. We have embedded the analysis into a renormalization group framework, using the SRG as a convenient tool to change the scale. This enables us to separately study the impact of scale changes on all the ingredients of the calculation. We are particularly interested in kinematic regions of experimental interest where these changes are significant.

For such regions we found that working at low resolution can have distinct advantages. We found that at high Q^2 ($Q^2 \approx 1.8\,\mathrm{GeV}^2$) and large x_d ($x_d > 1.5$), the local decoupling of the final state in the evolved picture leads to decreased contributions from final-state interactions and thereby an increased validity of the impulse approximation. We also saw that the explanation of factorization in the

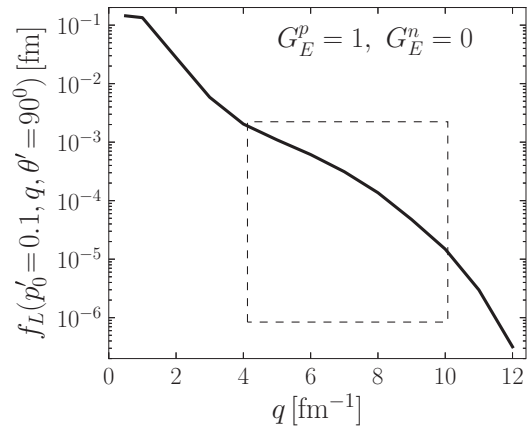

FIG. 20. Demonstration that f_L is a strong function of q. Y axis is the denominator of the ratio plotted in Fig. 19. For the region in which the ratio of f_L plateaus, the denominator by itself varies by over three orders of magnitude.

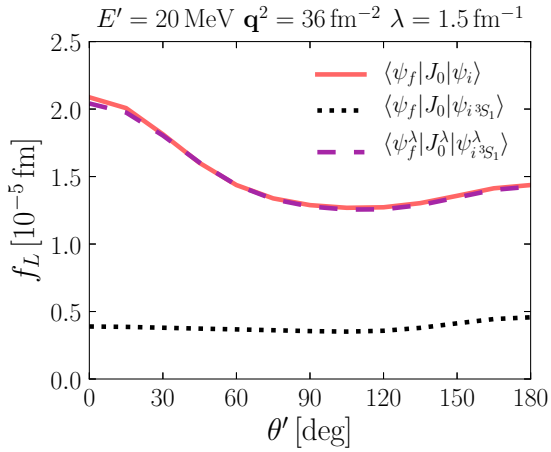

FIG. 21. Contribution to f_L from the deuteron S state in the evolved and unevolved case. Here $x_d = 1.88$, $Q^2 = 1.3\,\mathrm{GeV}^2$.

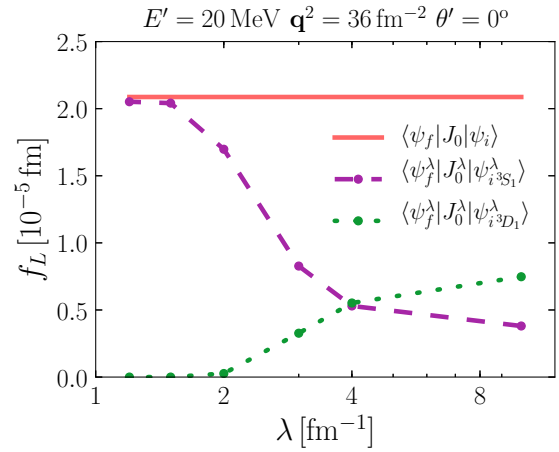

FIG. 22. Contribution to f_L from the deuteron S and D states as a function of SRG λ for the same x_d and Q^2 as in Fig. 21 but with fixed $\theta' = 0^\circ$.

observable f_L becomes straightforward in the low-momentum picture.

It is conventional wisdom that the low-resolution potentials are ill suited for high-momentum-transfer reactions, such as those used to probe short-range correlations in nuclei. By focusing on a particular kinematics region with large momentum transfer q^2 and relatively small energy E' ($Q^2 = 1.3\,\mathrm{GeV}^2$, $x_d = 1.88$), we demonstrated that this is not the case. We showed that the relevant RG changes to the operator are tractable, which allows us to recover the unevolved answer in the low-resolution picture.

Analysis of a reaction calculation often involves understanding which components of the nuclear wave functions are probed. For example, it might be claimed that a reaction is sensitive to the D-state probability in the deuteron. In our model calculations, such a claim would be based on the unevolved wave functions in Figs. 3 and 4, where we find that for intermediate momenta that the D-state deuteron wave function has a higher magnitude than the S-state wave function. However, as we saw in Fig. 4, the high-momentum part of the deuteron wave functions depends on the SRG scale. Therefore, the claim that a certain kinematics is sensitive to a specific channel in the deuteron wave function is highly scale dependent.

We see a representative demonstration of this in Fig. 21 using the kinematics explored in Sec. III D. The solid line in Fig. 21 is f_L in the unevolved case. The dotted line is f_L calculated by keeping only the S state in the deuteron. Thus keeping only the S state is clearly a very poor approximation in the unevolved case. However, as indicated by the dashed line, it is a very good approximation for the evolved case.

Figure 22 shows the contribution to f_L for $\theta' = 0^\circ$ from the S and D channels of the deuteron as a function of λ. We see that the S-channel contribution increases with SRG evolution, while the D-channel contribution is driven to zero. We stress that the results in Figs. 21 and 22 change quantitatively with different kinematics. Nonetheless, they demonstrate how an "intuitive" picture of probing specific parts of the nuclear wave function is highly scale dependent.

It has been established previously that the D-state probability of the deuteron, which is analogous to a spectroscopic factor, is not measurable [42,43]. We have seen how this is manifested in deuteron electrodisintegration as a scale dependence under SRG evolution. Our example demonstrates that if one tries to calculate the cross section at a definite high-resolution scale with a calculation that is not fully consistent, one would come to the false conclusion that this D-state physics is a measurable ingredient of the experiment rather than a scale- and scheme-dependent feature.

Thus our results supply an object lesson for those seeking to extract absolute nuclear structure information from knock-out reactions. In a simple picture at high RG resolution based on the IA, the cross section for the specified kinematics and a one-body current comes dominantly from high-momentum components of the deuteron wave function and the D-state part plays an essential role. Thus, one imagines the reaction is a probe of short-range correlations and the impact of the tensor force in nuclei. One also finds that final-state interactions are a critical ingredient, which generally obscures what is learned. But an analysis of the same kinematics at low RG resolution yields a very different picture of the cross section, which instead comes dominantly from simple wave functions and a two-body current well represented as contact operators. This picture implies a simple calculation of the identical cross section that does not rely on the D-state part of the deuteron wave function at all.

The results we have found from explicit calculations can be understood using simple, intuitive arguments. Schematic pictures of the dominant mechanisms for two classes of kinematics are shown in Fig. 23. Recall that we are in the center-of-mass (c.m.) system of the final proton and neutron, so their momenta are always back-to-back and equal in magnitude. For convenience we focus on scattering angle $\theta = 0$ and consider only the photon coupling to the proton, but the arguments here are easily generalized. In the initial state, the photon three-momentum and the net momenta in the deuteron must sum to zero, but we need to identify the

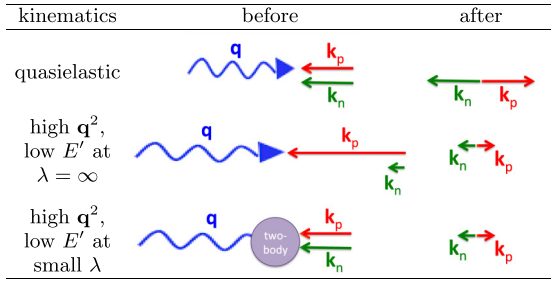

FIG. 23. Schematic pictures of the most important incoming and outgoing proton and neutron momenta for $\theta' = 0^\circ$ scattering in the impulse approximation with quasifree kinematics at any λ, and analogous pictures for scattering with large momentum transfer near threshold at high and low resolution.

dominant region of proton-neutron phase space for the cross section.

The first row in Fig. 23 illustrates the generic situation for quasifree kinematics and a one-body current. The definition of the quasifree ridge dictates the final magnitudes of momenta, equal to half the initial photon three-momentum. The one-body current J_0 by assumption couples only to the proton, so the neutron momentum is the same in the initial and final states while the proton gets exactly turned around. That implies that the initial nucleons have a small relative momentum, which is dominated by the relative S wave and is unchanged under RG evolution, implying that there will be little dependence on SRG λ on the quasifree ridge.

The other example, shown for high resolution on the second line and for low resolution on the third line, is the case we have considered in detail with large momentum transfer q^2 and relatively small final energy E'. The latter dictates the same low-relative-momentum final configuration for each resolution, but the dominant mechanism is forced to be very different. At high resolution, the one-body current mechanism requires a high-momentum proton (in that frame), which implies a high relative momentum—in other words, an SRC configuration. There are no such SRCs at low resolution, but there is an induced short-range two-body current, which mostly just stops low-relative-momentum nucleons in the deuteron. In the former case, the D state plays a dominant role (at least for intermediate momenta) while in the latter it is mostly S state. This example shows again how the kinematics alone does not always uniquely determine what is probed in the reaction.

The present investigations are only the start of what is needed for a thorough treatment of scale and scheme dependence for nuclear processes. Extensions include adding two-body currents, applications to few-body systems, consistent construction of operators for processes of interest from the RG perspective, and connecting to other knock-out processes. While these are technically much more complex, we expect that many of the basic physics observations will carry over. An interesting follow-up will be to examine the scheme dependence that comes from the choice of SRG generator. An alternative to $G_s = T$ is to choose a form that block-diagonalizes the Hamiltonian with respect to a specified momentum scale $\Lambda_{\rm bd}$ [44,45]. This scheme decouples physics above and below $\Lambda_{\rm bd}$, but does not have the *local* decoupling properties that were important for the FSI simplifications observed here. Work on all of these extensions is in progress.

ACKNOWLEDGMENTS

We would like to thank A. Dyhdalo, K. Hebeler, S. König, and D. Phillips for useful discussions. This work was supported in part by the National Science Foundation under Grants No. PHY-1306250, No. PHY-1404159, and No. PHY-1614460, the NUCLEI SciDAC Collaboration under DOE Grants No. DE-SC0008533 and No. DE-SC0008511, and the Double-Beta Decay and Fundamental Symmetries Topical Collaboration under DOE Grant No. DE-SC0015376.

APPENDIX: KINEMATIC VARIABLES TRANSFORMATION

The analysis of electron scattering on nuclei is often presented using the Lorentz-invariant kinematic variables Bjorken x and the virtual photon four-momentum squared, $Q^2 \equiv -q^2$ [13]. We note that x and Q^2 provide a complete kinematic specification for inclusive scattering from an unpolarized target but not (exclusive) deuteron electrodisintegration, although there is a one-to-one mapping between the center-of-mass variables[5] $(E', \mathbf{q}^2_{\rm c.m.})$ and (x, Q^2), which we provide below. The relative angle θ' of the outgoing proton relative to the photon provides us additional information in the deuteron electrodisintegration case. For example, in the impulse approximation θ' directly specifies which part of the deuteron wave function is probed. The θ' dependence is integrated over in the inclusive case.

The generalized Bjorken x_A for an A-body nuclear target is given by

$$x_A = \frac{Q^2}{2q \cdot P_A} A, \tag{A1}$$

where q^μ is the virtual photon four-momentum and P_A^μ is the four-momentum of the target nucleus. The range of x_A is $0 \leqslant x_A \leqslant A$, with $x_A = 1$ characterizing elastic scattering. For a deuteron target in the laboratory frame,

$$x_d = \frac{Q^2}{\omega_{\rm lab} M_d}, \tag{A2}$$

where M_d is the mass of the deuteron.

Given E' and $\mathbf{q}^2_{\rm c.m.}$, we can evaluate Q^2 in the center-of-mass frame,

$$Q^2 = \mathbf{q}^2_{\rm c.m.} - \omega^2_{\rm c.m.}, \tag{A3}$$

and use

$$\omega_{\rm c.m.} = E' + 2\,M_{np} - \sqrt{M_d^2 + \mathbf{q}^2_{\rm c.m.}}, \tag{A4}$$

where M_{np} is the average neutron-proton mass. To evaluate x_d from Eq. (A2), we express $\omega_{\rm lab}$ in terms of center-of-mass

[5] In other sections for notational brevity we set $\mathbf{q}^2_{\rm c.m.} \equiv q^2$. Here we keep the subscript c.m. to avoid any ambiguities.

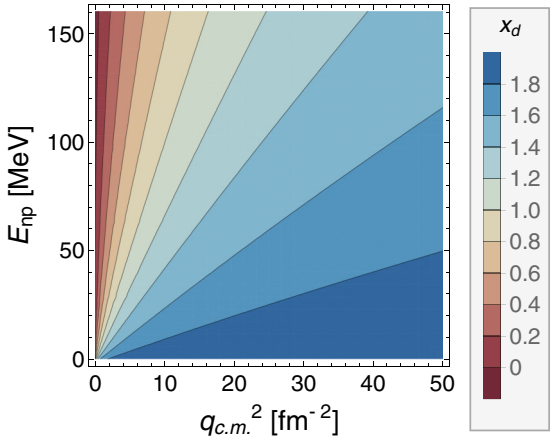

FIG. 24. Q^2 values as a function of E' and $\mathbf{q}^2_{\text{c.m.}}$.

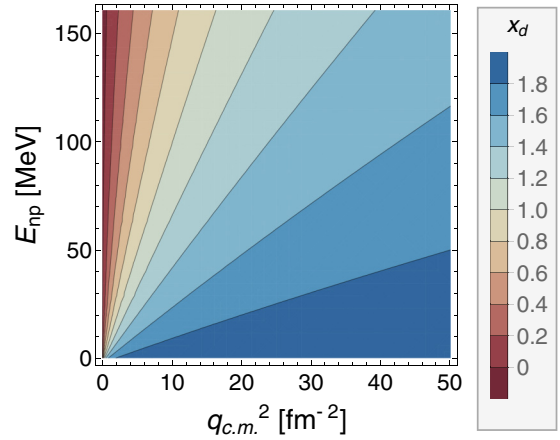

FIG. 25. x_d values as a function of E' and $\mathbf{q}^2_{\text{c.m.}}$.

quantities [40],

$$\omega_{\text{lab}} = \frac{E_d^{\text{c.m.}}}{M_d}\left(\omega_{\text{c.m.}} + \frac{\mathbf{q}^2_{\text{c.m.}}}{E_d^{\text{c.m.}}}\right), \tag{A5}$$

where $E_d^{\text{c.m.}}$ is the deuteron energy in the center-of-mass frame of the outgoing particles given by

$$E_d^{\text{c.m.}} = \sqrt{\mathbf{q}^2_{\text{c.m.}} + M_d^2}. \tag{A6}$$

Using Eqs. (A2), (A3), and (A5), we can map the c.m. variables to the Lorentz-invariant variables. The corresponding values for Q^2 and x_d as functions of E' and $\mathbf{q}^2_{\text{c.m.}}$ are shown in Figs. 24 and 25. The kinematically allowed regions are $Q^2 \geqslant 0$ and $0 \leqslant x_d \leqslant 2$.

[1] R. J. Furnstahl and A. Schwenk, J. Phys. G **37**, 064005 (2010).
[2] R. J. Furnstahl, in *Proceedings, International Conference on Nuclear Theory in the Supercomputing Era (NTSE-2013), Ames, Iowa, USA, May 13-17, 2013*, edited by A. M. Shirokov and A. I. Mazur (Pacific National University, Khabarovsk, 2014), p. 371.
[3] G. Sterman, J. Smith, J. C. Collins, J. Whitmore, R. Brock, J. Huston, J. Pumplin, W.-K. Tung, H. Weerts, C.-P. Yuan, S. Kuhlmann, S. Mishra, J. G. Morfín, F. Olness, J. Owens, J. Qiu, and D. E. Soper, Rev. Mod. Phys. **67**, 157 (1995).
[4] J. Collins, *Foundations of Perturbative QCD* (Cambridge University Press, Cambridge, UK, 2013).
[5] P. F. Bedaque and U. van Kolck, Annu. Rev. Nucl. Part. Sci. **52**, 339 (2002).
[6] E. Epelbaum, H.-W. Hammer, and U.-G. Meißner, Rev. Mod. Phys. **81**, 1773 (2009).
[7] R. Machleidt and D. R. Entem, Phys. Rep. **503**, 1 (2011).
[8] E. Epelbaum and U.-G. Meissner, Annu. Rev. Nucl. Part. Sci. **62**, 159 (2012).
[9] S. K. Bogner, R. J. Furnstahl, and A. Schwenk, Prog. Part. Nucl. Phys. **65**, 94 (2010).
[10] M. Alvioli, C. Ciofi Degli Atti, L. P. Kaptari, C. B. Mezzetti, and H. Morita, Int. J. Mod. Phys. **E22**, 1330021 (2013).
[11] J. Ryckebusch, W. Cosyn, and M. Vanhalst, J. Phys. G **42**, 055104 (2015).
[12] C. C. d. Atti, Phys. Rep. **590**, 1 (2015).
[13] O. Hen, G. A. Miller, E. Piasetzky, and L. B. Weinstein, Rev. Mod. Phys. **89**, 045002 (2017).
[14] R. Furnstahl, Nucl. Phys. Proc. B Suppl. **228**, 139 (2012).
[15] T. Duguet, H. Hergert, J. D. Holt, and V. Somà, Phys. Rev. C **92**, 034313 (2015).
[16] E. Braaten and L. Platter, Phys. Rev. Lett. **100**, 205301 (2008).
[17] J. Hofmann, M. Barth, and W. Zwerger, Phys. Rev. B **87**, 235125 (2013).
[18] S. K. Bogner, R. J. Furnstahl, and R. J. Perry, Phys. Rev. C **75**, 061001 (2007).
[19] R. J. Furnstahl and K. Hebeler, Rep. Prog. Phys. **76**, 126301 (2013).
[20] S. Binder, J. Langhammer, A. Calci, and R. Roth, Phys. Lett. B **736**, 119 (2014).
[21] R. Roth, A. Calci, J. Langhammer, and S. Binder, Phys. Rev. C **90**, 024325 (2014).
[22] R. Roth, A. Calci, J. Langhammer, and S. Binder, Few Body Syst. **55**, 659 (2014).
[23] M. D. Schuster, S. Quaglioni, C. W. Johnson, E. D. Jurgenson, and P. Navrátil, Phys. Rev. C **90**, 011301(R) (2014).
[24] T. Neff, H. Feldmeier, and W. Horiuchi, Phys. Rev. C **92**, 024003 (2015).
[25] T. Neff and H. Feldmeier, arXiv:1610.04066.
[26] N. M. Parzuchowski, S. R. Stroberg, P. Navrátil, H. Hergert, and S. K. Bogner, Phys. Rev. C **96**, 034324 (2017).
[27] H. Hergert, S. K. Bogner, J. G. Lietz, T. D. Morris, S. J. Novario, N. M. Parzuchowski, and F. Yuan, In-medium similarity renormalization group approach to the nuclear many-body problem, in *An Advanced Course in Computational Nuclear Physics: Bridging the Scales from Quarks to Neutron Stars*, edited by M. Hjorth-Jensen, M. P. Lombardo, and U. van Kolck (Springer International Publishing, Cham, Switzerland, 2017), pp. 477–570.
[28] S. Bacca and S. Pastore, J. Phys. G **41**, 123002 (2014).

[29] P. Navrátil, S. Quaglioni, G. Hupin, C. Romero-Redondo, and A. Calci, Phys. Scr. **91**, 053002 (2016).
[30] S. N. More, S. König, R. J. Furnstahl, and K. Hebeler, Phys. Rev. C **92**, 064002 (2015).
[31] C.-J. Yang and D. R. Phillips, Eur. Phys. J. A **49**, 122 (2013).
[32] B. Dainton, R. J. Furnstahl, and R. J. Perry, Phys. Rev. C **89**, 014001 (2014).
[33] R. B. Wiringa, V. G. J. Stoks, and R. Schiavilla, Phys. Rev. C **51**, 38 (1995).
[34] A. M. Mukhamedzhanov and A. S. Kadyrov, Phys. Rev. C **82**, 051601 (2010).
[35] A. Gezerlis, I. Tews, E. Epelbaum, M. Freunek, S. Gandolfi, K. Hebeler, A. Nogga, and A. Schwenk, Phys. Rev. C **90**, 054323 (2014).
[36] E. Epelbaum, H. Krebs, and U. G. Meißner, Phys. Rev. Lett. **115**, 122301 (2015).
[37] M. Piarulli, L. Girlanda, R. Schiavilla, R. N. Pérez, J. E. Amaro, and E. R. Arriola, Phys. Rev. C **91**, 024003 (2015).
[38] D. R. Entem, R. Machleidt, and Y. Nosyk, Phys. Rev. C **96**, 024004 (2017).
[39] E. R. Anderson, S. K. Bogner, R. J. Furnstahl, and R. J. Perry, Phys. Rev. C **82**, 054001 (2010).
[40] W. Fabian and H. Arenhovel, Nucl. Phys. A **314**, 253 (1979).
[41] S. K. Bogner and D. Roscher, Phys. Rev. C **86**, 064304 (2012).
[42] R. D. Amado, Phys. Rev. C **19**, 1473 (1979).
[43] J. L. Friar, Phys. Rev. C **20**, 325 (1979).
[44] E. Anderson, S. K. Bogner, R. J. Furnstahl, E. D. Jurgenson, R. J. Perry, and A. Schwenk, Phys. Rev. C **77**, 037001 (2008).
[45] N. M. Dicaire, C. Omand, and P. Navratil, Phys. Rev. C **90**, 034302 (2014).